Gomez Socola and Rodrigues
Earth, Planets and Space (2022) 74:185
https://doi.org/10.1186/s40623-022-01743-x

Earth, Planets and Space

TECHNICAL REPORT

Open Access

ScintPi 2.0 and 3.0: low-cost GNSS-based monitors of ionospheric scintillation and total electron content

Josemaria Gomez Socola and Fabiano S. Rodrigues*

Abstract

We have devoted efforts to the development and performance evaluation of new low-cost ionospheric instruments for studies that require distributed observations and for educational and citizen science initiatives. Here, we report results of some of these efforts. More specifically, we describe the design of new ionospheric sensors based on Global Navigation Satellite System (GNSS) receivers and single-board computers. The first sensor (ScintPi 2.0) is a multi-constellation, single-frequency ionospheric scintillation monitor. The second sensor (ScintPi 3.0) is a multi-constellation, dual-frequency ionospheric scintillation and total electron content (TEC) monitor. Both sensors were created using Raspberry Pi computers and off-the-shelf GNSS receivers. While they are not intended to fully replace commercial ionospheric monitors, they cost a fraction of their price and can be used in various scientific applications. In addition to describing these new sensors, we present examples of observations made by ScintPi 3.0 deployed in Presidente Prudente, Brazil (22.12 S, 51.41 W, − 17.67° dip latitude). These examples show the ability of our system to detect scintillation events and TEC depletions such as those associated with equatorial plasma bubbles. Additionally, our observations were made in parallel with a commercial receiver (Septentrio PolaRx5S), which allowed an evaluation of the scintillation and TEC measurements provided by our system. The comparison shows that ScintPi 3.0 can provide estimates of the amplitude scintillation index (S_4) and TEC that are in excellent agreement with those provided by PolaRx5S. We also show an example of the application of ScintPi 3.0 in distributed observations of ionospheric irregularities and scintillation over South America.

Keywords: Ionosphere, Scintillation, Total electron content, TEC, Monitor, Scintpi, Raspberry pi, GNSS, Low cost

*Correspondence: fabiano@utdallas.edu

The University of Texas at Dallas, Richardson, TX, USA

Graphical Abstract

Introduction

The variability of the Earth's ionosphere is an important component of space weather. From a fundamental point-of-view, the ionosphere can be described as a collisional, weakly magnetized plasma containing a wide range (in scale size and amplitude) of naturally occurring perturbations and interesting phenomena (Stubbe and Hagfors, 1997). For instance, we seek a better understanding of observed variations in morphology, composition, and thermal structure. We also would like to understand in more details the ionospheric responses to solar events such as coronal mass ejections (CMEs), solar flares and solar eclipses (e.g., Burns et al. 2007; Tsurutani et al. 2009; Verhulst and Stankov 2020; Zhang et al. 2021). Additionally, we also seek to advance our understanding of the ionospheric response to events occurring on the Earth's surface and at lower atmospheric altitudes that include earthquakes, tornadoes, and tsunamis (e.g., Nishioka et al. 2013; Komjathy et al. 2016).

From an applied point-of-view, the study of the ionosphere is equally interesting and challenging. This comes from the fact that the ionosphere affects the propagation of radio waves used for communication, navigation, and remote sensing (Basu et al. 1988; Carrano et al. 2012; Zhang and Morton 2009). For instance, the ionospheric plasma causes an additional delay to the travel time of radio signals used by global navigation satellite systems (GNSS). GNSS can be described as a satellite constellation that provides positioning, navigation and timing services. In addition to the Global Positioning System (GPS) operated by the United States, other GNSS constellations such as GLONASS (Russia), Galileo (European Union) and BeiDou (China) also exist and are widely used.

The ionospheric delay in the GNSS signals is closely related to ionospheric plasma density and, therefore, ionospheric variations can affect GNSS performance. Additionally, ionospheric plasma instabilities create a broad spectrum in scale sizes (from cm to several 10 s of km) of ionospheric irregularities (Fejer and Kelley, 1980). Irregularities with scale sizes around the Fresnel scale can cause strong diffraction of trans-ionospheric radio signals which, as a result, produce severe signal fading, commonly referred to as ionospheric scintillation (Yeh and Liu, 1982).

While ionospheric effects can be detrimental to various applications, they can also provide an opportunity for remote sensing techniques. Of particular interest here are refraction and diffraction effects. The frequency-dependent refractive index of the ionosphere allows, for instance, the use of signals of different frequencies and coherently transmitted by satellites to be employed in deriving information about the ionosphere. The difference in delay of the two signals is linearly related to the integral of the electron number density (in m^{-3}) along the signals' propagation path, which is commonly referred to as total electron content (TEC; 1×10^{16} electrons/$m^2 = 1$ TEC unit = TECU). Additionally, scintillation can be utilized to monitor and study ionospheric irregularities. For the case of L-Band (1–2 GHz) signals such as those used in GNSS, scintillation can be an indicator of irregularities with a few 100 s of m scale sizes.

The use of these effects for ionospheric remote sensing is well recognized. GNSS-based scintillation and TEC radio sensors, for example, have been widely used in fundamental and applied studies of the ionosphere (Van Dierendonck et al. 1993; Beach and Kintner, 2001; Skone

et al. 2001; Ledvina et al. 2003; de Paula et al. 2003a; Mitchel and Spencer, 2003; Aquino et al. 2009; O'Hanlon et al. 2011; Datta-Barua et al. 2015; Deshpande et al. 2012; Vani et al. 2019; Portella et al. 2021). Currently, Septentrio provides PolaRx5S (Septentrio, 2022) which can be described as a state-of-the-art multi-frequency, multi-constellation ionospheric monitoring GNSS reference receiver. PolaRx5S provides, among other parameters, high-rate (typically 50 Hz but 100 Hz also possible) information about the signal phase and amplitude, and real-time outputs of TEC values and scintillation indices. It also provides a comprehensive software package that allows users to set the receiver to a wide variety of applications.

Here, we present results of our efforts aimed at creating alternative low-cost ionospheric scintillation and TEC using inexpensive off-the-shelf GNSS receivers. This is a follow up of the work presented by Rodrigues and Moraes, (2019). The main goal of our efforts is to create an ionospheric monitoring system that is easy to deploy and operate, and whose cost is only a fraction of the commercial counterparts. Our monitor does not intend to fully replace a commercial monitor. It can assist, however, studies that require a large number of spatially distributed ionospheric observations and whose total cost would be prohibitive if using commercial receivers. Additionally, the simplicity of the system allows for easy deployment and operation and engagement of students in educational and research activities.

This presentation is organized as follows: In "Instrumentation" Section, we provide information about the two GNSS-based sensors (ScintPi 2.0 and ScintPi 3.0) which have been designed and prototyped. We also provide information about the Septentrio PolaRx5S receiver whose measurements are used in a comparative analysis. In "Deployment and observations" Section, we provide information about the deployment of ScintPi 3.0 in Presidente Prudente, Brazil, a site located near the southern peak of the equatorial ionization anomaly. In "Results and discussion" Section, we present and discuss examples of scintillation and TEC measurements made by ScintPi 3.0 and comparisons with measurements made by the collocated PolaRx5S receiver. We also present an example of observations made by three ScintPi 3.0 receivers used to monitor low-latitude ionospheric irregularities and scintillation over South America. "Summary and concluding remarks" Section summarizes our main results and conclusions.

Instrumentation

As mentioned earlier, this work was motivated by the results presented by Rodrigues and Moraes (2019). They developed and tested an inexpensive (~US$ 100.00) GPS-based ionospheric scintillation monitor (ScintPi). ScintPi is based on the Adafruit Ultimate GPS peripheral connected to a Raspberry Pi (RPi). Its development was intended for basic ionospheric research, education and citizen science initiatives. Rodrigues and Moraes (2019) showed that the signal-to-noise ratio (SNR) values output by the Adafruit receiver could be used as a proxy of the signal intensity. More importantly, they showed that the Adafruit output could be used to estimate the S_4 index. S_4 is an amplitude scintillation metric widely used in fundamental and applied studies of scintillation (Yeh and Liu, 1982). It can be defined as the standard deviation of the signal intensity (I) normalized by the average intensity:

$$S_4 = \sqrt{\frac{\langle I^2 \rangle - \langle I \rangle^2}{\langle I \rangle^2}} \quad (1)$$

where the angle brackets represent ensemble averaging. In practice, time averages are used. Specialized scintillation monitors typically compute S_4 values using measurements at 50–100 Hz sampling rates made over time intervals of 60 s (e.g., Van Dierendonck et al. 1993; Beach and Kintner, 2001; O'Hanlon et al. 2011).

Observations made by ScintPi in parallel with a Septentrio PolaRx5S receiver allowed the authors to evaluate ScintPi and to determine the strengths and weaknesses of the system. In particular, they found that the low sampling rate (10 Hz) and low resolution of SNR values (1 dB) output by the Adafruit GPS receiver did not affect the ability of the system to adequately detect scintillation and determine its severity. However, they found that the Adafruit had a threshold in the SNR output at 52 dB. This means that any values greater than 52 dB would be output by the receiver as 52 dB. That would affect the ability of the system to properly detect scintillation at high elevation angles when the SNR of the signals could reach values close to 52 dB or more.

In an effort to create better ionospheric monitors while maintaining their reduced cost, we investigated the use of other off-the-shelf GNSS receivers for scintillation as well as TEC measurements. The communication with the receiver and acquisition of data remained to be done by a Raspberry Pi 3 Model B+(1.4 GHz 64-bit quad-core ARM Cortex-A53 CPU and 1 GB LPDDR2 SDRAM) with a 64 GB SD card. The tests led to us to identify two receivers that satisfied our necessities. These receivers were used to create ScintPi 2.0 and ScintPi 3.0, which are described below. The first version of ScintPi published by Rodrigues and Moraes (2019) is now referred to as ScintPi 1.0. Figure 1 shows the three versions of ScintPi monitors we have developed.

The overall hardware setup for ScintPi 2.0 and 3.0 follows that of ScintPi 1.0, which is illustrated in Fig. 2.

Fig. 1 The three versions of ScintPi ionospheric monitors. ScintPi 1.0 was described by Rodrigues and Moraes (2019). ScintPi 2.0 and 3.0 are introduced in this report

Fig. 2 Diagram illustrating the main components and connections of a ScintPi monitor

Each system consists of an external active GNSS antenna, GNSS receiver, Raspberry Pi (RPi) and connections. The GNSS antenna is connected to the receiver through a Radio-Frequency (RF) cable. The antenna provides the GNSS signal to the receiver. DC power is also provided by the receiver to the active antenna through the RF connection. The receiver is then connected to the RPi via one of its USB ports. The USB connection allows data from the receiver to be sent to the RPi. It also allows the RPi to provide DC power to the receiver. Note that ScintPi 1.0 uses a GPS-only receiver and a GPS antenna can be used instead of more expensive GNSS antenna.

ScintPi 2.0

ScintPi 2.0 is the result of our first effort to improve ScintPi 1.0. The main objective leading to the development of ScintPi 2.0 was to find an alternative receiver without the limiting 52 dB SNR threshold of the Adafruit Ultimate GPS receiver. In ScintPi 1.0 we read National Marine Electronics Association (NMEA) standard messages sent by the receiver and used the values in the SNR field as an indicator of signal strength (Rodrigues and Moraes, 2019).

ScintPi 2.0 was developed using u-blox SparkFun GPS Breakout—NEO-M9N which features the u-blox M9 GNSS chip. The receiver does not have the same 52 dB SNR limitation of the Adafruit GPS receiver. More importantly, while the cost of the NEO-M9N receiver (US$ 64.95) is somewhat higher than that of the Adafruit Ultimate GPS receiver (US$ 39.95), it is capable of receiving signals from multiple GNSS satellites. More specifically, the receiver is capable of tracking the following signals: GPS L1 C/A, QZSS L1 C/A/S, GLONASS L10F, BeiDou B1I and Galileo E1B/C. Additionally, the receiver is capable of tracking the following L1 C/A signals from Satellite-Based Augmentation Systems (SBAS): WAAS, EGNOS, MSAS, GAGAN. Additionally, the receiver provides signal strength, (carrier-to-noise ratio—C/N0) values at a rate as high as 20 Hz (when tracking signals from 4 GNSS constellations). The Adafruit Ultimate GPS receiver provided SNR values at a rate of 10 Hz. The resolution of the signal strength values provided by the M9 chip is the same as the Adafruit receiver, that is, 1 dB. Therefore, ScintPi 2.0 can be described as a low-cost single-frequency (~ 1.6 GHz) GNSS-based ionospheric scintillation monitor.

ScintPi 3.0

During our search for alternatives to the Adafruit Ultimate GPS receiver, we also tested dual-frequency GNSS

options. While they were significantly more expensive than the NEO-M9N, they could provide new parameters, that is, scintillation measurements in two frequencies and estimates of the ionospheric TEC. Our tests of receivers and comparison of measurements made by commercial monitors led us to develop ScintPi 3.0.

ScintPi 3.0 was developed using u-blox SparkFun GPS Breakout—ZED-F9P (US$ 275.00) which features the u-blox 184-channel u-blox F9 engine (u-blox, 2021b). It provides, however, C/N0 values with resolution of 1 dB for two signals (at ~ 1.2 GHz and 1.6 GHz) transmitted by satellites from different GNSS constellations being tracked. More specifically, it provides information for the following signals: GPS L1C/A and L2C, GLONASS L1OF and L2OF, GALILEO E1B/C and E5b, BEIDOU B1I and B2I, QZSS L1C/A as well as L1S and L2C, and SBAS L1C/A (in more recent versions). The receiver can provide C/N0 values at rate as high as 25 Hz depending on the number of GNSS constellations being tracked. The resolution of the SNR values is the same of ScintPi 1.0 and 2.0, that is, 1 dB.

Additionally, ZED-F9P also provides carrier phase (ϕ) and pseudo-range (ρ) information for each signal being tracked. We used this information to estimate the total electron content (TEC) along the path between ScintPi 3.0 and satellites:

$$\mathrm{TEC} = \int_{RX}^{TX} N_e(s)ds \tag{2}$$

where $N_e(s)$ represents the electron density along the path (s) between ScintPi 3.0 (RX) and the satellite (TX). Given measurements at two frequencies f_1 and f_2, TEC can be estimated from pseudo-ranges and phase measurements (Jakowski et al. 2011):

$$\mathrm{TEC}_\phi \approx \frac{1}{40.3}\left(\frac{f_1^2 f_2^2}{f_1^2 - f_2^2}\right)(\phi_1 - \Phi_2) \tag{3}$$

$$\mathrm{TEC}_\rho \approx \frac{1}{40.3}\left(\frac{f_1^2 f_2^2}{f_1^2 - f_2^2}\right)(\rho_2 - \rho_1) \tag{4}$$

where the subscripts in Eqs. 3 and 4 refer to frequency, and the phase values are in meters. TEC_ϕ and TEC_ρ are referred to as code TEC and phase TEC, respectively. The frequencies observed by ScintPi 3.0 are around 1.6 GHz and 1.2 GHz and, for simplicity, are referred here as L1 and L2. Of particular importance to our development and applications of interest are phase TEC measurements, which provide precise but relative (due to phase ambiguity) TEC estimates. Nevertheless, we also compute and present results of code TEC, which is a noisy estimate of TEC but, given corrections of satellite and receiver biases, can provide absolute TEC values.

Given the information above, ScintPi 3.0 can be described as a low-cost dual-frequency GNSS-based ionospheric scintillation and TEC monitor. Table 1 lists approximate costs of the parts used to build ScintPi 2.0 and 3.0.

Table 1 List of main parts used to build ScintPi 2.0 and 3.0 and approximate costs

Part	Approximate cost (US$)	
	ScintPi 2.0	ScintPi 3.0
Raspberry Pi 3 Model B+	35.00	35.00
64 GB micro-SD card	15.00	15.00
Raspberry Pi power supply	8.00	8.00
Raspberry Pi case	11.00	11.00
Micro USB cable (Receiver to Raspberry Pi)	10.00	10.00
u-blox SparkFun GPS Breakout—NEO-M9N	65.00	
u-blox SparkFun GPS Breakout—ZED-F9P		275.00
GNSS Antenna*	155.00	155.00
Coaxial cable and connectors (Antenna to Receiver)	55.00	55.00
Approximate total cost of parts	354.00	564.00

Note that the price of GNSS antennas can vary significantly, from only a few 10 s to 1000 s of US$. The price listed here is for a GNSS antenna made by Abracon LLC (model AEAGMK148060-S1575), which we successfully used in our installs of ScintPi 2.0 and 3.0

Table 2 Location of ScintPi 3.0 receivers whose data is used in this study

Site	Latitude	Longitude	Dip latitude
Presidente prudente—PPR	22.12°S	51.41°W	− 17.67°
Campina grande—CG	7.21°S	35.91°W	− 10.25°
Jicamarca radio observatory—JRO	11.95°S	76.88°W	− 1.38°

Software and setup

The u-blox receivers output data following a proprietary binary format called UBX, which groups the data into different UBX messages. Software written in C language has been created to run in the Raspberry Pi that is part of ScintPi 2.0 and ScintPi 3.0. The software reads the receiver messages and retrieves information that is of interest to ionospheric studies. The information listed in Table 2 includes time, coordinates of the receivers, information about satellite positions (azimuth and elevation angles), SNR, phases, and pseudo-ranges. The software also outputs formatted data files with relevant information at 10 Hz sampling rate. The Raspberry Pi models used to develop ScintPi 2.0 and 3.0 are equipped

with wired and wireless internet capabilities. The high-rate observations used in this report were stored locally and transferred to a server at UT Dallas once a day using the remote sync (rsync) utility. Scintillation indices and TEC are generated after processing the high-rate data collected by the monitors. Each prototype generated a relatively large amount of data (~0.7 GB for ScintPi 2.0 and ~2 GB for ScintPi 3.0) per day requiring an adequate internet connection for data transfer.

Deployment and observations

After tests in our lab in 2019 and 2020 we deployed prototypes of ScintPi 2.0 and 3.0 at a few sites in South America for field tests. The deployments at low latitudes allow us to evaluate the performance of the monitors at varying scintillation and TEC conditions. For instance, since early 2021 we have operated different setups of ScintPi 2.0 and ScintPi 3.0 at the Jicamarca Radio Observatory (JRO) which is located near the magnetic equator. While different setups (data acquisition modes) were tested, the hardware have yet to fail.

More recently, however, we were given the opportunity to deploy a ScintPi 3.0 in Presidente Prudente—PPR (22.1°S, 51.24°W, − 16.8° dip latitude) near the southern crest of the equatorial ionization anomaly in Brazil. The system was deployed in parallel (using a signal splitter) with a commercial scintillation and TEC monitor (Septentrio PolaRx5S). Therefore, the collocated deployment allowed us to better evaluate the performance of ScintPi 3.0 with respect to this widely used commercial monitor. The location near the equatorial anomaly peak also allowed us to evaluate the performance of ScintPi 3.0 under a wide range of scintillation conditions. The measurements in PPR were made using a PolaNt Choke Ring B3/E6 antenna and a Tallysman TW150 L-Band/GNSS signal splitter.

Here we present and discuss examples of scintillation and TEC measurements made by the ScintPi 3.0 deployed in PPR. We must remind the reader that ScintPi 2.0 uses a single-frequency model of the u-blox family of GNSS receivers. The S4 L1 measurements provided by ScintPi 2.0 are virtually the same as those provided by ScintPi 3.0. Therefore, to avoid repetition we focus on ScintPi 3.0 measurements in this report. The system made measurements at a sampling rate of 10 Hz collecting signal parameters from four different constellations: GPS, GLONASS, GALILEO and BeiDou. The measurements to be presented and discussed here were made on Dec. 27 and Dec. 28, 2021. These days were selected because ScintPi 3.0 shows the occurrence of scintillation over a wide range of intensities and the occurrence of TEC depletions. Additionally, collocated measurements made on this day by a Septentrio PolaRx5S were also available for this study.

Septentrio PolaRx5S

PolaRx5S is defined by Septentrio as the world's leading ionospheric GNSS receiver (Septentrio, 2022). It provides estimates of amplitude and phase scintillation as well as TEC using signals from various GNSS constellations. The signals available for measurements depend on the GNSS tracking that have been enabled when purchasing the receiver. The monitor in Presidente Prudente can make triple-frequency measurements of the signals transmitted by GPS, GLONASS, GALILEO and BeiDou.

PolaRx5S and its antecessor (PolaRxS) are commonly used for observations of ionospheric scintillation and TEC in fundamental and applied studies (Moraes et al. 2018; Vani et al. 2021; de Paula et al. 2021). The PolaRx5S installed in Presidente Prudente uses a PolaNt Choke Ring B3/E6 antenna. This is a high precision multi-frequency antenna for reference stations. The antenna is equipped with low-noise amplifiers and is designed to mitigate multipath by attenuating reflected signals. Default settings for GNSS signal processing were used for the Septentrio PolaRx5S, ScintPi 2.0 (NEO-M9N) and ScintPi 3.0 (ZEP-F9P) measurements presented in this study.

Complementary measurements

We will also present initial results that demonstrate the usefulness of ScintPi 3.0 in distributed monitoring and studies of ionospheric irregularities and scintillation. For that purpose, we will also show measurements made by ScintPi 3.0 deployed at JRO in Peru and Campina Grande in Brazil. Instead of Choke Ring antennas, the monitors at these sites used Abracon LLC GNSS antennas (model AEAGMK148060-S1575). The Abracon antenna was selected after testing different models of antennas. Using spaced measurements, we found that the Abracon antenna performed exceptionally well compared with the PolaNt antenna. We do anticipate, however, that the Abracon antenna will not be able to mitigate the effects of multipath effects as well as the PolaNt Choke Ring can in situations where multipath is unavoidable. The antennas at JRO and Campina Grande, however, were adequately installed to maximize field of view (no obstructions around) and to minimize the effects of multipath. Table 2 summarizes the locations of these sensors.

Results and discussion

Amplitude scintillation measurements

We start by presenting examples and results of our evaluation amplitude scintillation measurements. Figures 3, 4

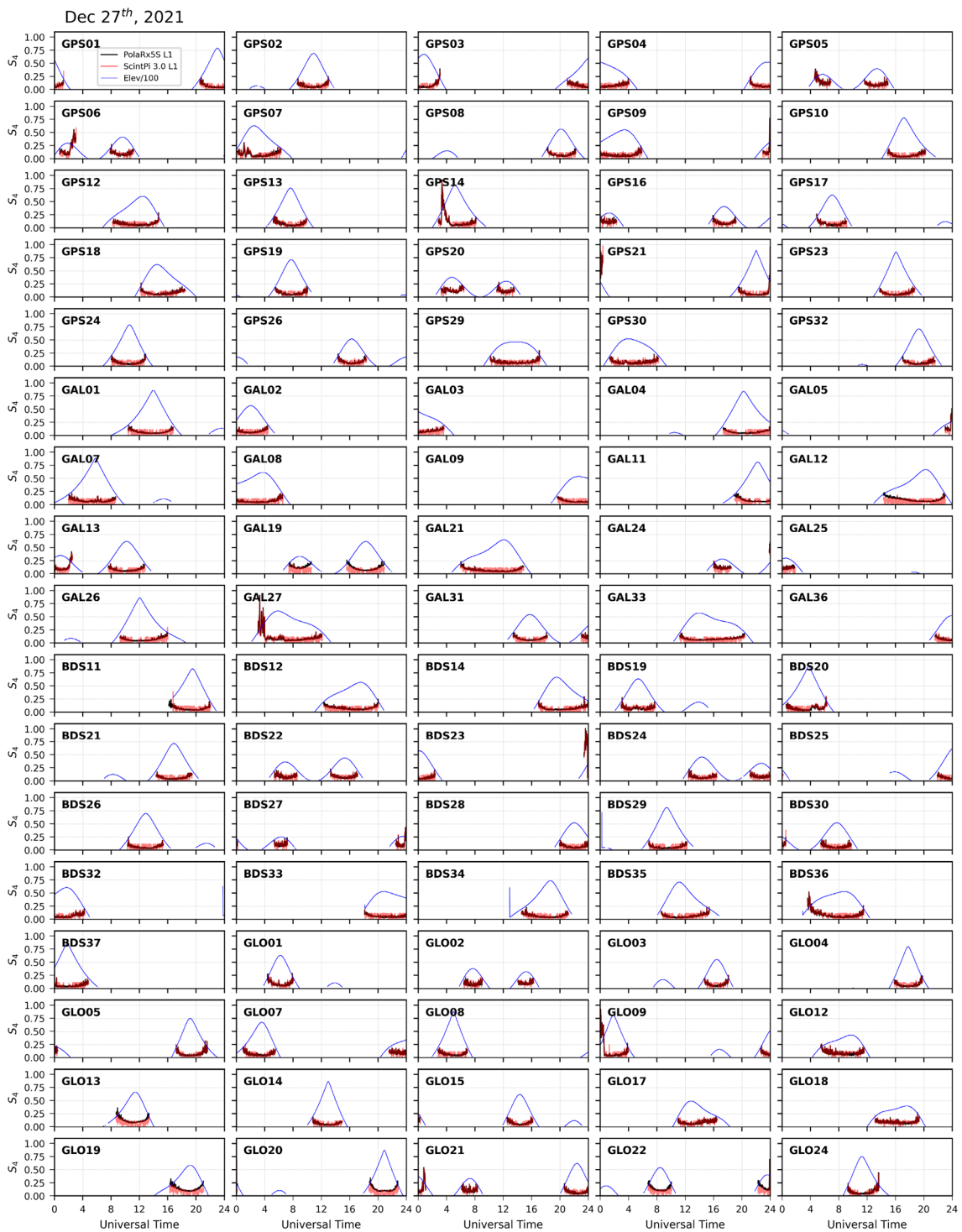

Fig. 3 Summary of L1 (~ 1.6 GHz) S_4 measurements made by ScintPi 3.0 (red curves) and collocated Septentrio PolaRx5S (black curves) on December 27, 2021. These monitors were collocated in Presidente Prudente (PPR), Brazil. The blue curves represent satellite elevation angles. The constellation and satellite identifier number are indicated in each panel

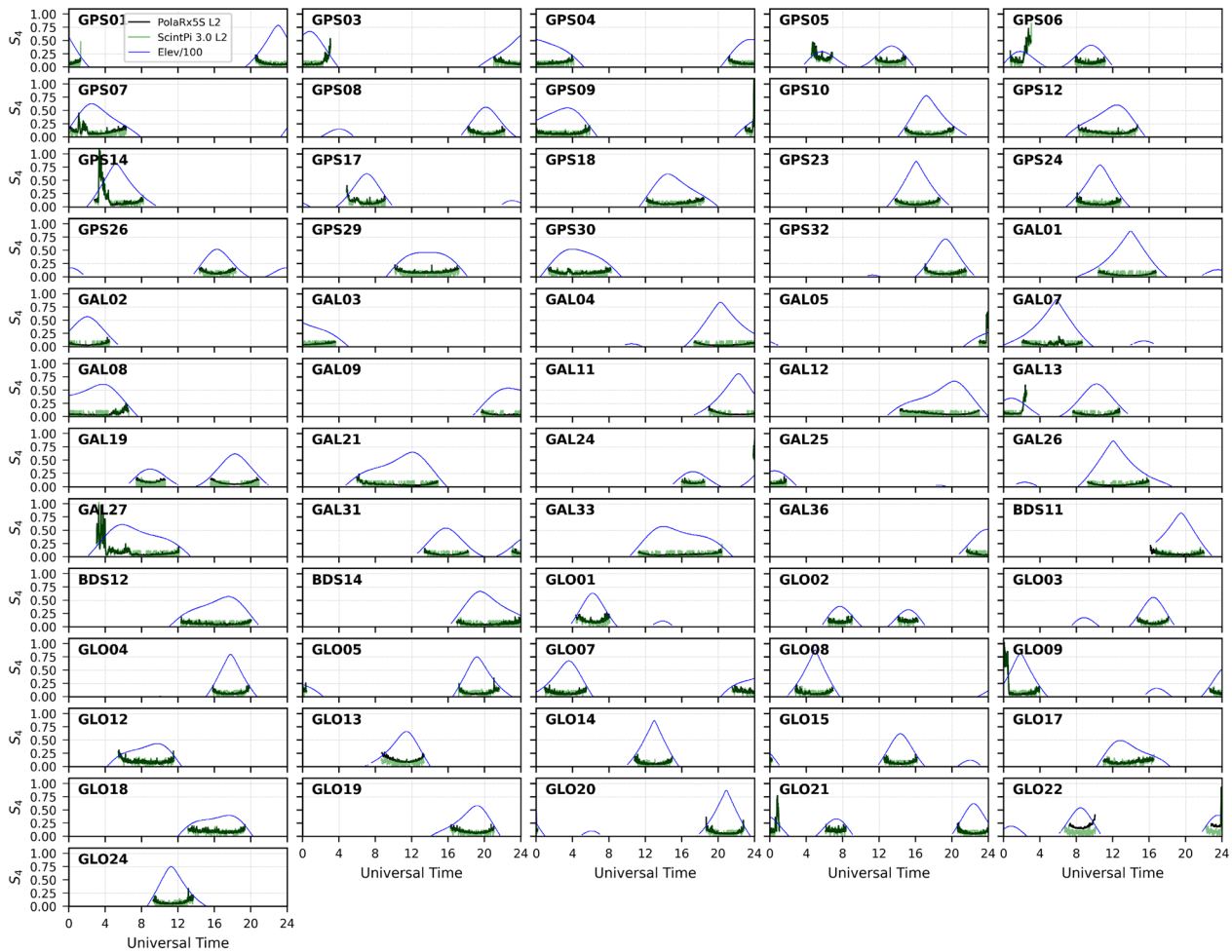

Fig. 4 Summary of L2 (~ 1.2 GHz) S_4 measurements made ScintPi 3.0 (green curves) and Septentrio PolaRx5S (black curves) on December 27, 2021. These monitors were collocated in Presidente Prudente (PPR), Brazil. The blue curves represent satellite elevation. The constellation and satellite identifier number are indicated in each panel

show examples of typical amplitude scintillation measurements made by ScintPi 3.0 and comparisons with collocated PolaRx5S records considering GNSS L1 and L2 signals, respectively. As mentioned earlier, these measurements were made at the Presidente Prudente site, in the southeastern Brazilian region.

Figure 3 shows (red curves) the amplitude scintillation index (S_4) for the L1 (~ 1.6 GHz) signals measured by ScintPi 3.0 on Dec. 27, 2021. More specifically, it shows the temporal variation of the S_4 values for each satellite tracked throughout the day. Each panel corresponds to the records from one satellite, and its constellation and identifier number are indicated in the upper left portion of the panel. Each panel also shows the elevation (blue curve) of the satellite. Only data for satellites with elevation > 20° are shown. Finally, S_4 data from PolaRx5S are also shown in each panel for comparison purposes.

Figure 4 shows the S_4 values for the L2 (~ 1.2 GHz) signals measured by ScintPi 3.0 (green curves) and Septentrio on Dec. 27, 2021. The format is the same as that of Fig. 3. Figures 3, 4 serve to illustrate that the S_4 values provided by ScinPi 3.0 follow very closely the those provided by the Septentrio monitor. Careful inspection of the measurements shown in Figs. 3, 4 shows that increases in S_4 values only occur during nighttime hours, mostly between approximately 00:00 UT (21:00 LT) and 04:00 UT (01:00 LT). This agrees with the expectation of scintillation associated with equatorial plasma bubbles (EPBs) reaching low latitudes, as is the case of PPR. A closer look in the data and additional details will be provided in the following sections.

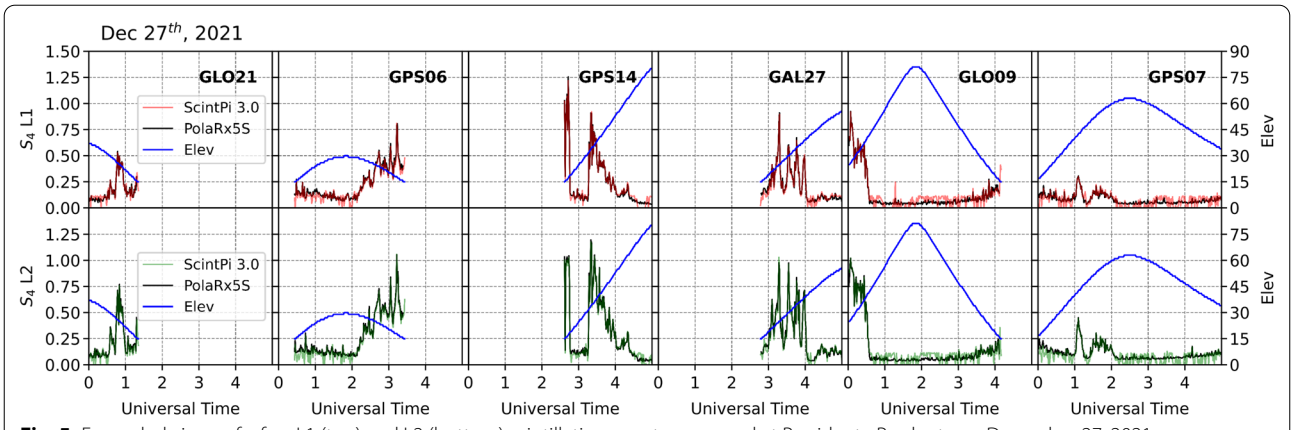

Fig. 5 Expanded views of a few L1 (top) and L2 (bottom) scintillation events measured at Presidente Prudente on December 27, 2021

For completeness, we also show expanded views of L1 and L2 scintillation measurements in Fig. 5. It shows a closer look at a few examples of scintillations measured by ScintPi 3.0 and PolaRx5S. Figure 5 allows one to better visualize the good agreement between the S_4 values provided by the two receivers. Similar to ScintPi 1.0 (Rodrigues and Moraes, 2019) low S_4 values ($S_4 < \sim 0.2$) provided by ScintPi 3.0 are more variable than those provided by PolaRx5S. This is because of the lower resolution of signal strength values provided by the u-blox receivers compared to PolaRx5S.

Next, to better quantify the agreement between the S_4 values provided by ScintPi 3.0 and those output by the Septentrio monitor, we provide the results presented in Fig. 6. Figure 6 shows scatter plots of the ScintPi S_4 versus Septentrio S_4 for L1 (red) and L2 (green) and for the two days of measurements (rows). Figure 6 also summarizes our comparisons of the measurements showing, for each day and signal, the coefficient of linear correlation (r), the average value (μ) and the standard deviation (σ) of ScintPi S_4 with respect to Septentrio S_4 values. Therefore, μ and σ represent the average and standard deviation, respectively, of the differences in S_4 values provided by ScintPi 3.0 with respect to S_4 values provided by the PolaRx5S. Only data from satellites with elevation angle greater than 20° are shown, and only data for which scintillation is observed (Septentrio $S_4 > 0.2$) are considered in the analyses. The results show that the ScintPi S_4 values are highly correlated with the Septentrio values with r ranging from 0.968 to 0.981. The results also show that the deviation of ScintPi 3.0 values with respect to Septentrio are minimal, with the average values ranging between 0.020 and 0.039 and the standard deviation ranging between 0.042 and 0.070.

Total electron content (TEC) measurements

We now turn our attention to TEC measurements made by ScintPi 3.0. In the following sections, we present and discuss code and phase TEC measurements made by ScintPi 3.0 and a comparison of these measurements with similar observations made by the collocated Septentrio monitor. Example results include TEC depletions detected by our ScintPi 3.0 and associated with scintillation events, and estimates of the temporal variation of vertical TEC curves.

Examples of code and phase TEC measurements

Figure 7 shows a summary of line-of-sight (slant) TEC measurements made by ScintPi 3.0 on Dec. 27, 2021. It shows, more specifically, the local variation of the TEC measurements obtained from differential pseudo-ranges (code TEC, TEC_ρ) in gray as well as from differential phase (phase TEC, TEC_ϕ) measurements in red. The observations are shown for all satellites capable of transmitting two signals (L1 and L2) and tracked by ScintPi 3.0 throughout the day. The constellation and satellite identifier numbers are indicated in each panel. For reference, the satellite elevation angle (blue curve) is also indicated in each panel.

As mentioned earlier, code TEC is a noisy but absolute measurement. Phase TEC, on the other hand, is a relative measurement because of the intrinsic ambiguities associated with carrier phase tracking. Phase TEC measurements, however, are more precise than code TEC measurements (Jakowski, 1996). Figure 7 serves to show that both phase and code TEC can be estimated from ScintPi 3.0 measurements. For better visualization purposes, phase TEC curves were leveled to code curves to illustrate the agreement between the two estimates.

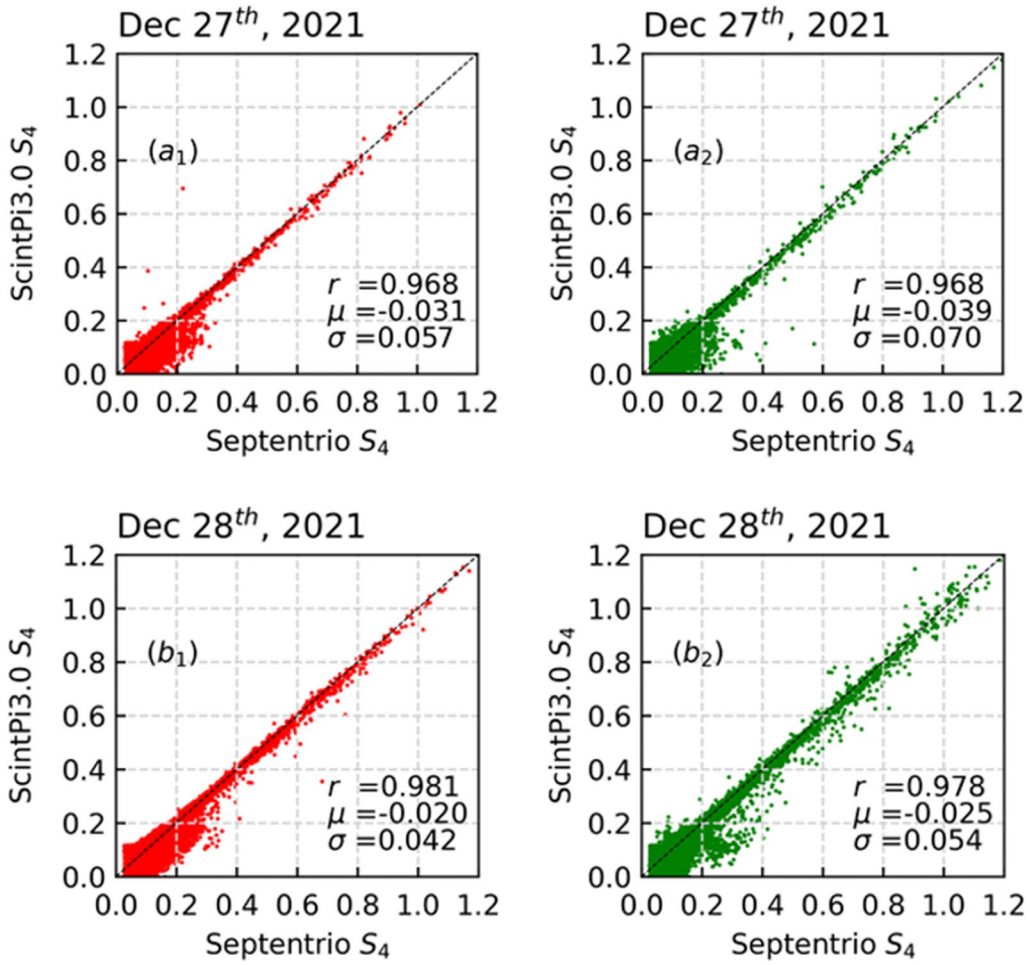

Fig. 6 Comparisons between S_4 values measured on December 27 and 28, 2021 by the ScintPi 3.0 and Septentrio PolaRx5S. These monitors were collocated in Presidente Prudente, Brazil. Comparisons for L1 (~ 1.6 GHz) signals are shown in panels (**a1**) and (**b1**), while comparisons for L2 signals (~ 1.2 GHz) are shown in panels (**a2**) and (**b2**). Each panel shows the coefficient of linear correlation (r), the average value ($\mu = \langle S_{4,Sci} - S_{4,Sep} \rangle$) and standard deviation (σ) of ScintPi 3.0 S_4 values with respect to Septentrio S_4 values

Figure 7 also exemplifies the fact that data from a large number of satellites (61 in this example) can be obtained with ScintPi 3.0. This allows for a wide coverage of the sky by a single station compared to GPS-only receivers.

Comparison with Septentrio TEC measurements

We now take a closer look at the TEC measurements provided by ScintPi 3.0 and compare them with measurements provided by the collocated Septentrio PolaRx5S monitor. The left-hand side panels in Fig. 8 show expanded views of code (gray) and phase TEC (red) example measurements made by ScintPi 3.0 on Dec. 27, 2021. Information about constellation and satellite identifier numbers are exhibited in the respective panels. For comparison, PolaRx5S measurements for the same satellites and signals are shown in the middle panels. Finally, for a more direct evaluation of ScintPi 3.0 observations, phase TEC measurements from ScintPi 3.0 and PolaRx5S are shown in the right-hand side panels. Figure 8 shows that, for some signals, code TEC provided by Septentrio is noticeably less noisy than the code TEC provided by ScintPi 3.0. This is typically the case of signals from Galileo. The same difference is not as noticeable for signals from GPS, GLONASS and BeiDou. Note that BeiDou has fewer satellites than other constellations and measurements were not available for the time window in Fig. 8. Differences in code TEC for ScintPi 3.0 and PolaRx5S are the result of different receiver hardware and signal processing. More importantly, Fig. 8 shows that the phase TEC provided by ScintPi 3.0 is in excellent agreement with the phase TEC provided by PolaRx5S. ScintPi 3.0 measurements can capture small amplitude (fraction

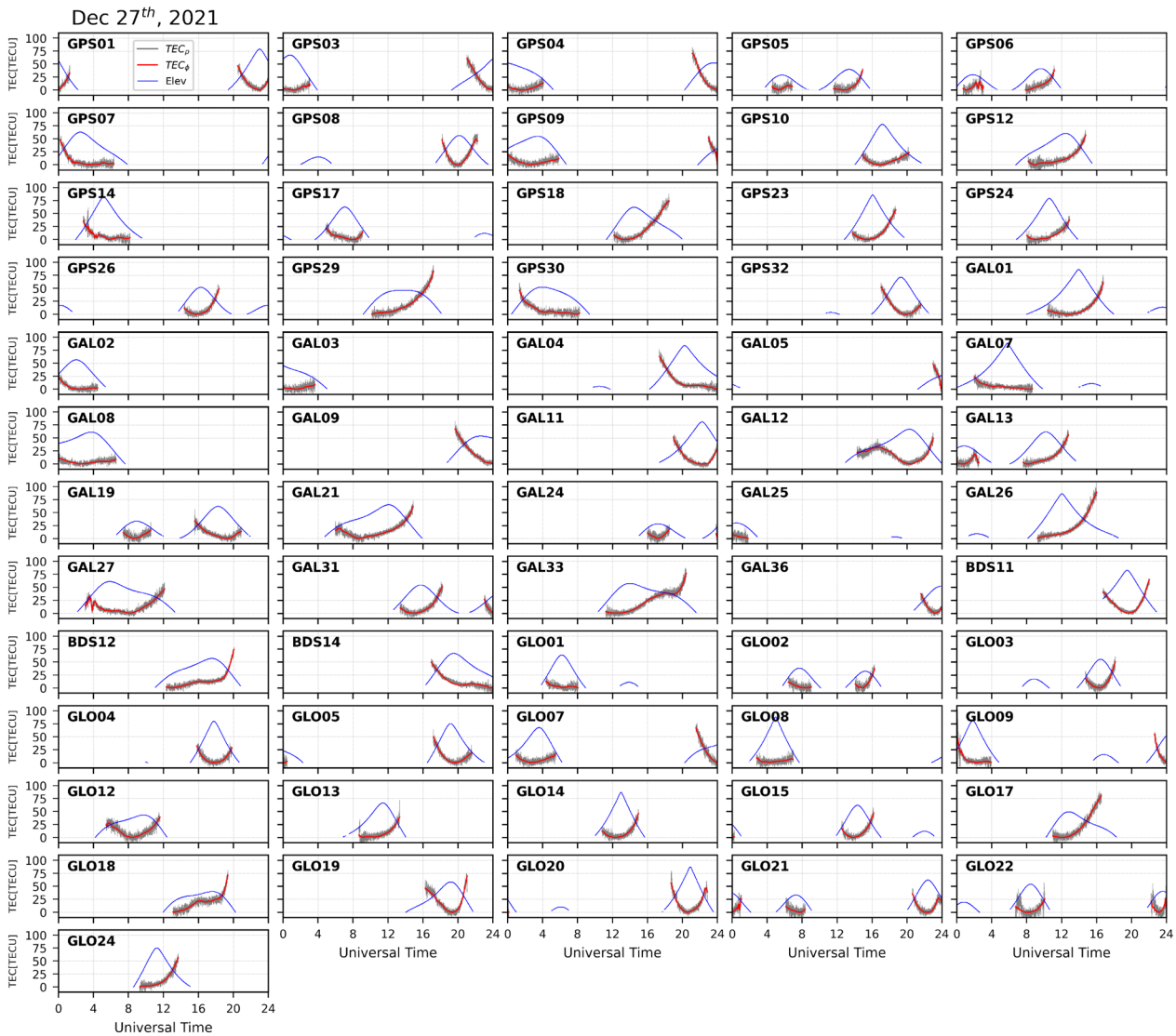

Fig. 7 Example of typical code TEC (gray curves) and phase TEC (red curves) estimates that can be obtained with ScintPi 3.0. Satellite elevation (blue curves) are also shown for reference

of TECU), long period (~1 h) variations as seen in the examples. ScintPi phase TEC measurements can also capture the large gradients associated with TEC depletions such as that detected by GAL27 between about 03:00 and 04:00 UT. Finally, because ScintPi 3.0 can make high-rate (up to 20 Hz) measurements of TEC, the system can be used to study small-scale irregularities.

While our initial goal was to produce sensors capable of providing information about the occurrence of amplitude fading cases in L-Band signals and about the occurrence of small-scale irregularities in TEC, we realized that ionospheric users might also be interested in the time variation of the vertical TEC for various applications.

We now present results that illustrate the potential of ScintPi 3.0 measurements on providing the temporal variation of absolute vertical TEC (VTEC). Again, for better evaluation purposes our ScintPi 3.0 results are presented alongside similar estimates produced using collocated Septentrio measurements in PPR. The estimation of absolute VTEC curves involves leveling the more precise but relative phase TEC to the absolute but noisy code TEC curves, taking into consideration the satellite differential code biases (DCBs) as well as the receiver DCBs, and applying a mapping function that converts slant TEC measurements to VTEC estimates. The procedure we followed is similar to that described by Carrano and

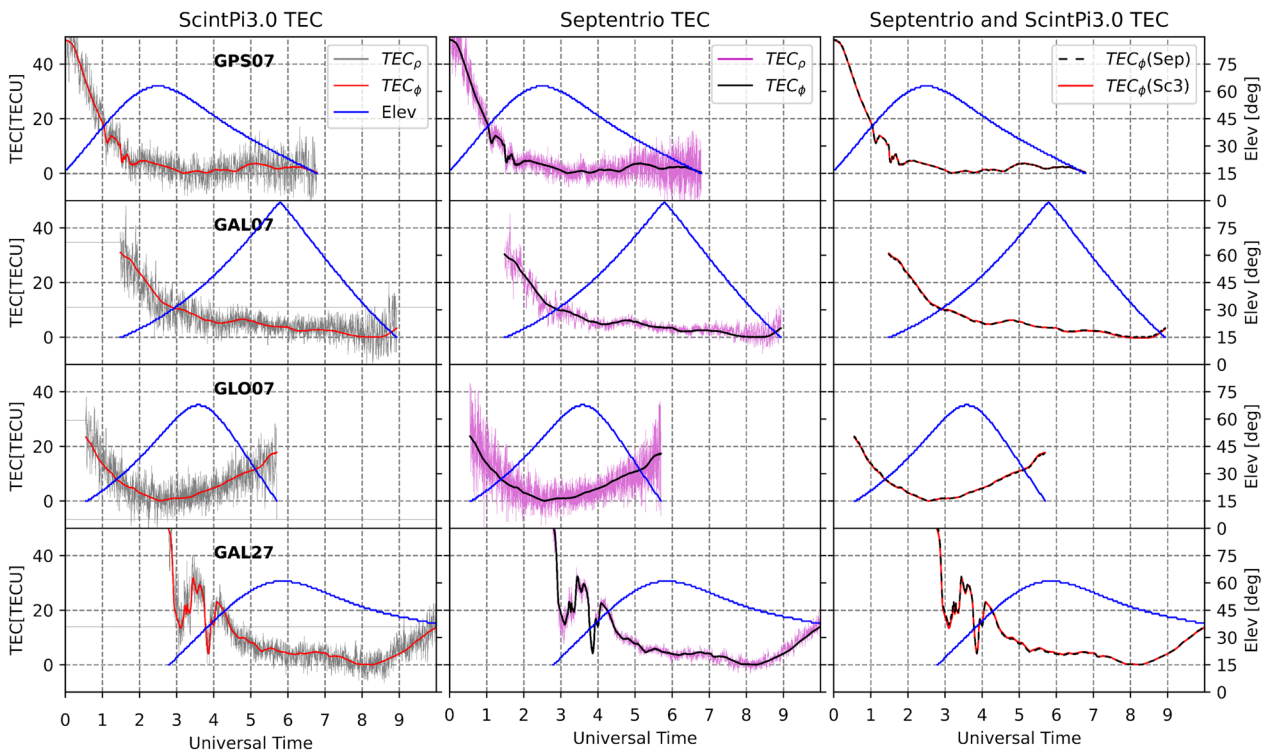

Fig. 8 Comparisons between code TEC and phase TEC measurements made on December 27, 2021 by ScintPi 3.0 and Septentrio PolaRx5S. These monitors were collocated in Presidente Prudente, Brazil

Groves (2006), except that we simply set the receiver bias as the value that causes the minimum observed VTEC near local sunrise to be zero for simplicity. Carrano and Groves (2006) propose and apply a more detailed and accurate approach to determine the receiver bias. We point out that we are not interested in the accuracy of the VTEC method at this time but, instead, how ScintPi 3.0 results compared to those from PolaRx5S. The satellite differential code biases (DCB) were obtained from the Crustal Dynamics Data Information System (CDDIS). Conversion of slant TEC to VTEC was done using the Single Layer Model (SLM) mapping function (Klobuchar, 1987; Carrano and Groves, 2006):

$$VTEC = TECcos\left[arcsin\left(\frac{R_E}{(R_E+h)}\cos(E)\right)\right] \qquad (5)$$

where E is the elevation angle of the GNSS satellite with respect to receiver, $h = 350$ km is the thin shell height, and R_E is the Earth's mean radius

Figure 9 shows an example of our results. The left-hand side panels show the VTEC derived from ScintPi 3.0 measurements of GPS (top) and GALILEO (bottom) signals. The right-hand side panels show the VTEC derived from the Septentrio signals. The most striking result is that the derived VTEC curves are virtually the same for signals from both monitors providing evidence of the usefulness of ScintPi 3.0 measurements in studies of the VTEC. Additionally, the measurements also show the same ionospheric behavior derived from measurements from distinct GNSS constellations, confirming the quality of the VTEC estimates provided by ScintPi 3.0. The GPS and GALILEO curves show maximum VTEC estimates of approximately 45 TECU around 1800 UT (~1500 LT) and minimum VTEC around 0800 UT (~0500 LT). The VTEC curves also show larger TEC variability during nighttime (2000 UT–0800 UT) which would be expected from the large latitudinal gradients in ionospheric density created by the pre-reversal enhancement (PRE) of the zonal electric field around sunset hours and by large electron density variations associated with equatorial plasma bubbles (Valladares et al. 2001). The results in Fig. 9 are also in good agreement with independent results presented by Okoh et al. (2021). Their estimates of TEC using u-blox F9P and comparisons with other non-collocated data sources led them to suggest that the receiver could be adequate for TEC studies.

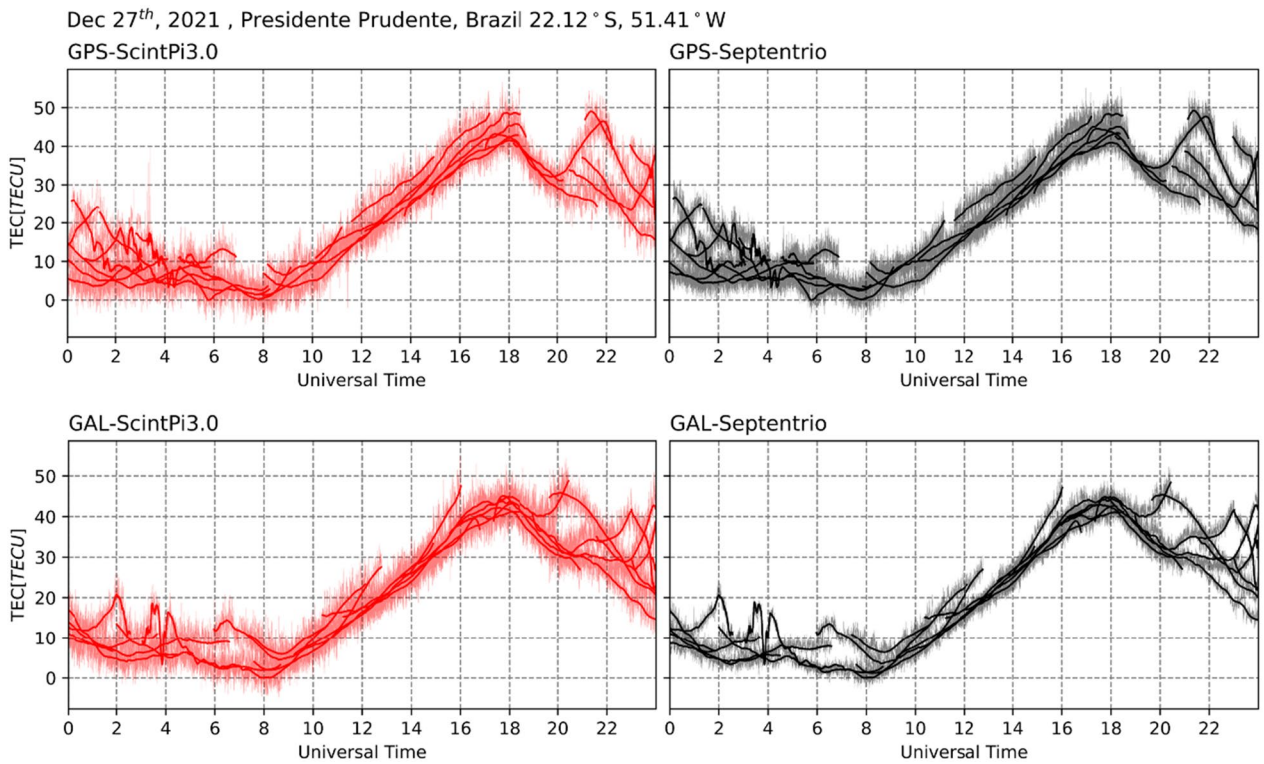

Fig. 9 Left panels: time variation of vertical TEC (VTEC) derived from ScintPi 3.0 measurements of GPS (top) and GALILEO (bottom) signals. Right panels: time variation of vertical TEC (VTEC) derived from PolaRx5S measurements of GPS (top) and GALILEO (bottom) signals

Example of application

One of the main motivations of our efforts towards the development of low-cost sensors was to increase the accessibility to measurements that would allow the monitoring as well as fundamental and applied studies of ionospheric irregularities and scintillation. Here, we show measurements that demonstrate the potential of ScintPi 3.0 to distributed monitoring and measurements of ionospheric TEC perturbations and scintillation associated with equatorial plasma bubbles. More specifically, we now present simultaneous measurements made by three ScintPi 3.0 monitors deployed in South America, at the Jicamarca Radio Observatory (JRO), Presidente Prudente (PPR) and Campina Grande (CG). Figure 10 shows the spatial and temporal distribution of the scintillation measurements made by these monitors. It shows the S_4 index on L1 signals (all constellations) as a function of ionospheric pierce point (IPP) coordinates. The color scale indicates the S_4 value on the L1 signals.

The measurements in Fig. 10 serve to show that a low-cost deployment such as that provided by ScintPi 3.0 (and 2.0) can allow the monitoring and detection of scintillation and irregularities over a wide region. The example shows clear occurrence of scintillation in Campina Grande (CG) and Presidente Prudente (PPR). No obvious enhancements in L1 S_4 could be observed at Jicamarca (JRO) and it was unclear from the scintillation observations alone that irregularities occurred. Closer inspection of S_4 along with TEC measurements can provide additional information as it will be shown later in this section.

The example in Fig. 10 also shows that moderate scintillation occurs first in CG, around 23:00 UT. Moderate and intense scintillation starts to occur around 01:00 UT in PPR. The observations reflect the fact that CG is located closer to the magnetic equator and to the east of PPR. The sunset terminator crosses the magnetic longitude sector of CG first, triggering the EPBs earlier. These EPBs reach CG quickly since the site is located near the equator, causing the first scintillation events.

The fact that PPR is located to the west of and at a higher magnetic latitude compared to CG can explain the occurrence of scintillation at a later time. Conditions for EPB generation (sunset terminator) would take longer to occur in the longitude sector of PPR. It would also take longer for EPBs to develop vertically, map along magnetic field lines and reach the latitude of PPR compared to CG. Additionally, one can see that strong scintillation events occur more often in PPR. This can be explained by the location of the site. The severity of amplitude scintillation increases with the amplitude of the ionospheric density

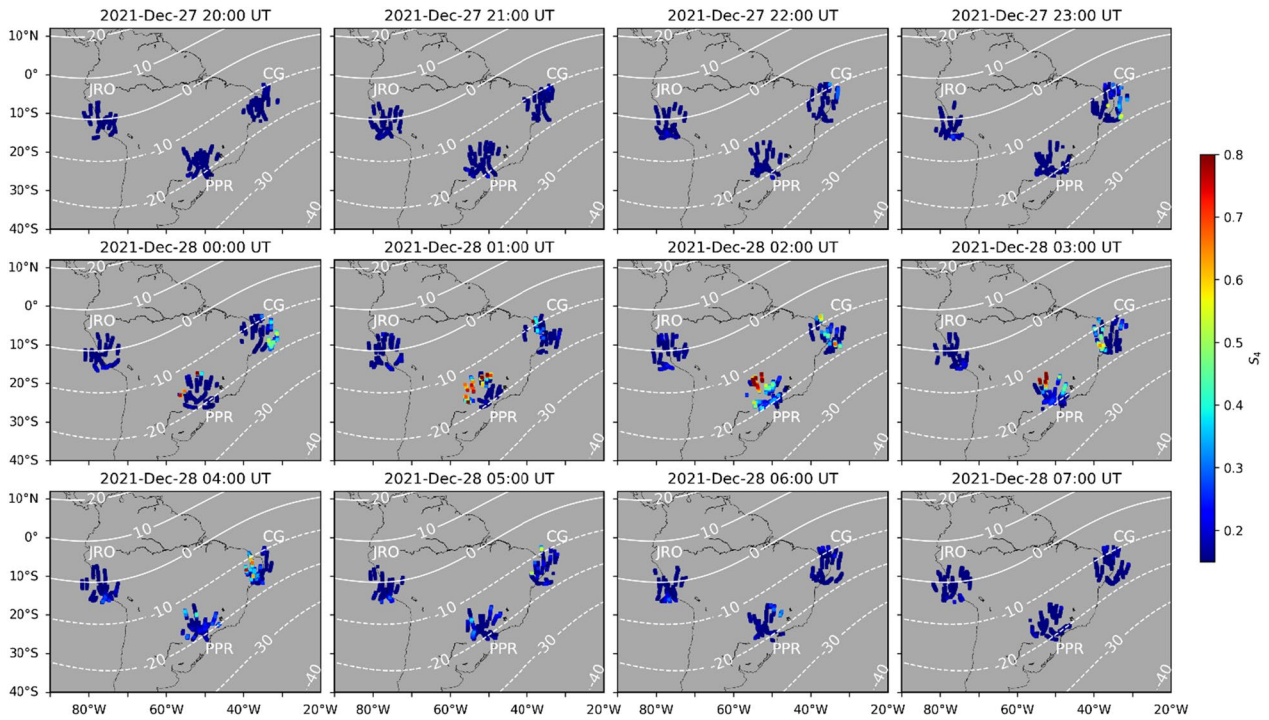

Fig. 10 Snapshots of L1 S_4 measurements as a function of ionospheric piercing point (IPP) coordinates for measurements made by ScintPi 3.0 sensors at the Jicamarca Radio Observatory (JRO), Campina Grande (CG), and Presidente Prudente (PPR). The time on top of each panel indicates the end time of the 1 h intervals under which measurements were made. Only measurements from satellites with elevation greater than 30° are shown

perturbations (Basu et al. 1976). PPR is located near the nominal location of the southern peak of the equatorial ionization anomaly where background densities are larger resulting in greater amplitudes of density perturbations. Those conditions are often invoked to explain the occurrence of stronger scintillation events near the equatorial anomaly peaks (de Paula et al. 2003b).

Figure 10 does not show moderate or strong scintillation events at Jicamarca. This can be caused by the absence of EPBs in the Western sector of South America or by the fact that ionospheric F-region densities near the equator are typically low leading to only weak or absent scintillation at L-Band signals. The TEC measurements provided by ScintPi 3.0 can provide additional information about the occurrence of EPBs.

Figure 11 shows an example of simultaneous measurements of TEC and scintillation made by the ScintPi 3.0 monitors at JRO (left panels), CG (middle panels) and PPR (right panels). The example serves to show signatures of ionospheric plasma depletions over the three sites. The depletions can be seen as large amplitude (several TECU) variations in TEC. The depletions are commonly accompanied by increases in scintillation activity (S_4 values) and short-time, small-amplitude variations in TEC. At JRO, in particular, it can be seen that scintillation did occur but only weakly between 01:00 and 02:00 UT associated with a TEC depletion and irregularities. Examples of EPBs over CG and PPR can be seen at 03:00–04:00 UT and 00:00–02:00 UT, respectively, with more noticeable TEC depletions and steeper S_4 increases. Therefore, the three monitors provide evidence of EPBs occurring throughout the American sector. Additionally, the measurements show that scintillation in the L2 signals (black curves) are stronger than the scintillations in the L1 signals (red curves). This is a result of amplitude scintillation scaling with frequency (Fremouw et al., 1978; Van Dierendonck et al. 1993; Carrano et al. 2014; Jiao and Morton, 2015).

The examples of measurements in Figs. 10, 11 serve to show that ScintPi 3.0 can aid studies of ionospheric irregularities and scintillation requiring distributed observations. While we do not envision ScintPi 3.0 fully replacing commercial receivers employed by arrays of distributed sensors such as the Low-latitude Ionosphere Sensor Network—LISN (Valladares and Chau, 2012) they can help to aid and expand these arrays.

One direct benefit of ScintPi 3.0 is the reduced cost of maintenance and replacement compared to commercial

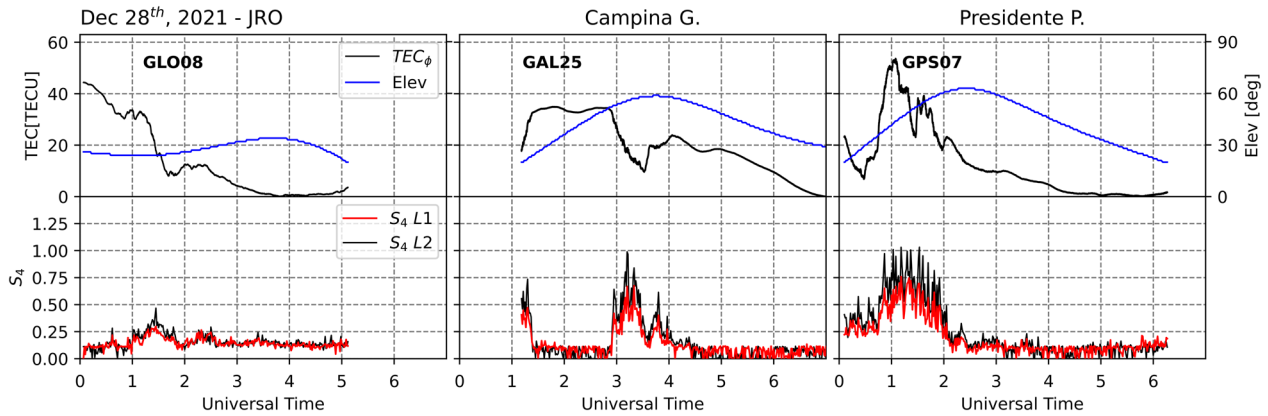

Fig. 11 Examples of TEC depletions (top) and amplitude scintillation at L1 and L2 signals (bottom) as measured by ScintPi 3.0 monitors located at JRO (left panels), CG (middle panels) and PPR (right panels) on December 28, 2021

monitors. A defective commercial monitor might need to be sent back to manufacturer creating expenses related to shipping and repair and extended downtime. ScintPi 3.0 can simply be fully replaced reducing costs and downtime.

Summary and concluding remarks

We reported results of our efforts related to the development and evaluation of new low-cost ionospheric instruments for studies that require distributed observations and for educational and citizen science initiatives. More specifically, we described the design, observations, and performance of new GNSS-based ionospheric sensors.

The first new sensor (ScintPi 2.0) is a multi-constellation, single-frequency ionospheric scintillation monitor. The second sensor (ScintPi 3.0) is a multi-constellation, dual-frequency ionospheric scintillation and total electron content (TEC) monitor. While ScintPi 2.0 can only be used for single-frequency (~ 1.5 GHz) studies of scintillation, its price is nearly half of that of ScintPi 3.0.

Both sensors were created using development boards (Raspberry Pi) and off-the-shelf GNSS receivers. While they are not intended to fully replace commercial ionospheric monitors, they cost a fraction of their price and can be used in various scientific applications. The low cost allows for a large number of monitors to be deployed providing larger coverages or increased spatial resolutions. Furthermore, a defective commercial monitor might need to be sent back to manufacturer creating expenses related to shipping and repair and interruption of observations. In the case of ScintPi 2.0 or 3.0, the monitors can be simply fully replaced at a low cost while causing reduced downtime in the observations. ScintPi sensors also feature built-in capability of internet connection, which allows them to provide real-time or near real-time information. In fact, there has been an effort to evaluate the ability of using distributed ScintPi 1.0 monitors to provide real-time information about scintillation activity over Brazil (Freitas et al. 2022).

To illustrate the capability of the new sensors, we presented examples of scintillation and TEC measurements made by a ScintPi 3.0 monitor deployed in Presidente Prudente, Brazil (22.1°S, 51.24°W,— 16.8° dip latitude). The measurements were made in parallel with a commercial scintillation and TEC monitor (Septentrio PolaRx5S) which allowed a direct evaluation of measurements provided by our system.

We showed that ScintPi 3.0 can detect amplitude scintillation at two frequencies (~ 1.2 and ~ 1.6 GHz) and provide S_4 index values that are in excellent agreement with those provided by the Septentrio monitor. The coefficient of linear correlation (r) between ScintPi 3.0 and PolaRx5S S_4 values is about 0.96–0.98. The root-mean-square error (σ) of the S_4 values provided by ScintPi 3.0 with respect to PolaRx5S varied between 0.04 and 0.07.

With respect to TEC measurements, we showed that ScintPi 3.0 can make measurements of TEC depletions such as those associated with ionospheric EPBs. ScintPi 3.0 phase TEC measurements match extremely well the phase TEC measurements provided by PolaRx5S. In addition to relative TEC measurements, we also showed that ScintPi 3.0 can provide absolute TEC observations which in turn can be used to determine the temporal variation of the vertical TEC (VTEC) near the observation site.

Finally, we showed examples of simultaneous scintillation and TEC measurements made by three ScintPi 3.0 monitors distributed over South America. The examples serve to illustrate the ability of the monitors to produce low-cost, easy to deploy and easy to maintain distributed

observations of ionospheric irregularities and scintillation. While ScintPi 3.0 is not intended to fully replace commercial monitors, it can be used to monitor scintillation and irregularities and to aid fundamental and applied studies that require low-cost instrumentation including arrays with a large number of sensors. While several scientific investigations can take advantage of ScintPi 3.0, we offer a couple of examples. For instance, the occurrence of mid-latitude scintillation and irregularities (e.g., Rodrigues et al. 2021) is expected to be reduced compared to low latitudes making it more difficult to justify the deployment and operation of an array of commercial high-rate scintillation and TEC monitors. An array of ScintPi 3.0, however, can be deployed over mid-latitudes to gain more insight on the spatial distribution and occurrence rates of mid-latitude ionospheric irregularities and scintillation, and about the underlying TEC conditions under which they develop at a reduced cost. An inexpensive local or regional array of ScintPi 3.0 can also be deployed to infer information about ionospheric Traveling Ionospheric Disturbances (TIDs), including propagation characteristics (e.g., Valladares and Hei, 2012).

The observations reported here show the occurrence of scintillation that is mostly moderate but with some intense cases at times. While we did not find evidence for concern related to measurements, future work will target a more comprehensive analysis of the ScintPi 2.0 and 3.0 performances, including the occurrence of loss of lock, under more severe scintillation conditions. This should provide additional insight on the performance of commercial (u-blox) GNSS receivers under scintillation conditions and insight on the performance of ScintPi 2.0 and 3.0 as ionospheric monitors.

Additionally, the reduced cost of ScintPi 3.0 allows its use in educational and citizen science initiatives. The results presented here are part of the graduate student work of one of the authors (JGS) at UT Dallas. The work of Freitas et al. (2022) exemplifies another graduate student project involving low-cost scintillation receivers (ScintPi 1.0). Additionally, UT Dallas undergraduate students have already been working on projects related to improving some of the hardware and software utilized by ScintPi monitors. One specific example is the work of Wright et al. (2022), which created an autonomous, solar-powered platform for ScintPi 3.0 that could be used in experiments or deployed by citizen scientists. The project allowed students to develop hard and soft skills. As part of the project, they worked as team and gained hands-on experience with hardware by designing, building, and deploying the system. The project also provided opportunities to gain experience and improve proficiency in computer languages. Additionally, the project allowed students to learn about space sciences and space weather, interpreting and presenting results.

Abbreviations

GPS: Global positioning system; GNSS: Global navigation satellite system; TEC: Total electron content; SNR: Signal-to-noise ratio; C/N0: Carrier-to-noise ratio.

Acknowledgements

Differential code biases (DCBs) were obtained through the online archives of the Crustal Dynamics Data Information System (CDDIS), https://cddis.nasa.gov/archive/gnss/products/bias/, NASA Goddard Space Flight Center, Greenbelt, MD, USA. The authors would like to thank Dr. Igo Paulino and Dr. Ricardo Buriti for hosting the ScintPi 3.0 in Campina Grande, Brazil. The authors also would like to thank the Jicamarca Radio Observatory for hosting another ScintPi 3.0. The Jicamarca Radio Observatory (JRO) is a facility of the Instituto Geofisíco del Perú operated with support from NSF Award AGS-1732209 through Cornell. Finally, the authors would like to thank UNESP, on behalf of I. Tsuchiya and J. F. Galera Monico for hosting a ScintPi 3.0 in Presidente Prudente and making the Septentrio PolaRx5S measurements available to this study. The PolaRx5S measurements were supported through the INCT GNSS-NavAer project, grants CNPq 465648/2014-2, FAPESP 2017/50115-0 and CAPES 88887.137186/2017-00.

Author contributions

FSR conceived the project, supervised the design and development of ScintPi 2.0 and 3.0 and analyses of the measurements, interpreted the results, and contributed to the writing of the manuscript. JGS carried out the development of ScintPi 2.0 and 3.0 and the analyses of the measurements, created the figures, and contributed to interpretation of the results and to the writing of the manuscript. Both authors read and approved the final manuscript.

Funding

This work was supported by UT Dallas start-up funds to FSR and NSF Award AGS- 2122639.

Availability of data and materials

Ionospheric scintillation and TEC data used in this study are available in the following public repository: https://doi.org/10.5281/zenodo.7384019.

Declarations

Ethics approval and consent to participate

Not applicable.

Consent for publication

Not applicable.

Competing interests

The authors declare that they have no competing interests.

Received: 15 April 2022 Accepted: 18 November 2022
Published online: 14 December 2022

References

Aquino M, Monico JFG, Dodson AH et al (2009) Improving the GNSS positioning stochastic model in the presence of ionospheric scintillation. J Geod 83:953–966. https://doi.org/10.1007/s00190-009-0313-6

Basu S, Basu S, Khan BK (1976) Model of equatorial scintillations from in-situ measurements. Radio Sci 11(10):821–832. https://doi.org/10.1029/RS011i010p00821

Basu S, MacKenzie E, Basu S (1988) Ionospheric constraints on VHF/UHF communications links during solar maximum and minimum periods. Radio Sci 23(3):363–378. https://doi.org/10.1029/RS023i003p00363

Beach TL, Kintner PM (2001) Development and use of a GPS ionospheric scintillation monitor. IEEE Trans Geosci Remote Sens 39(5):918–928. https://doi.org/10.1109/36.921409

Burns AG, Solomon SC, Wang W, Killeen TL (2007) The ionospheric and thermospheric response to CMEs: challenges and successes. J Atmos Solar-Terrestrial Phy 69(1–2):77–85. https://doi.org/10.1016/j.jastp.2006.06.010

Carrano CS, Groves KM, Caton RG (2012) Simulating the impacts of ionospheric scintillation on L band SAR image formation. Radio Sci. https://doi.org/10.1029/2011RS004956

Carrano CS, Groves K (2006) The GPS segment of the AFRL-SCINDA global network and the challenges of real-time TEC estimation in the equatorial ionosphere, proceedings of the 2006 national technical meeting of the institute of navigation Monterey, CA. p 1036–1047

Carrano CS, Groves KM, Delay SH, Doherty PH (2014) An inverse diffraction technique for scaling measurements of ionospheric scintillations on the GPS L1, L2, and L5 carriers to other frequencies. In proceedings of the 2014 international technical meeting of the institute of navigation. CA: Institute of Navigation. San Diego. p 709–719

Datta-Barua S, Su Y, Deshpande K, Miladinovich D, Bust GS, Hampton D, Crowley G (2015) First light from a kilometer-baseline Scintillation auroral GPS Array. Geophys Res Lett 42:3639–3646. https://doi.org/10.1002/2015GL063556

de Paula ER, Rodrigues FS, Iyer KN, Kantor IJ, Abdu MA, Kintner PM et al (2003) Equatorial anomaly effects on GPS scintillations in Brazil. Adv Space Res 31(3):749–754. https://doi.org/10.1016/S0273-1177(03)00048-6

de Paula ER, Rodrigues FS, Iyer KN, Kantor IJ, Abdu MA, Kintner PM, Ledvina BM, Kil H (2003) Equatorial anomaly effects on GPS scintillations in brazil. Adv Space Res 31(3):749–754. https://doi.org/10.1016/S0273-1177(03)00048-6

de Paula ER, Martinon ARF, Moraes AO, Carrano C, Neto AC, Doherty P et al (2021) Performance of 6 different global navigation satellite system receivers at low latitude under moderate and strong scintillation. Earth Space Sci. https://doi.org/10.1029/2020EA001314

Deshpande KB, Bust GS, Clauer CR, Kim H, Macon JE, Humphreys TE, Bhatti JA, Musko SB, Crowley G, Weatherwax AT (2012) Initial GPS scintillation results from CASES receiver at South Pole Antarctica. Radio Sci. https://doi.org/10.1029/2012RS005061

Dierendonck Van AJ, Klobuchar J, Hua Q (1993) "Ionospheric scintillation monitoring using commercial single frequency C/A code receivers," proceedings of the 6th international technical meeting of the satellite division of the institute of navigation (ION GPS 1993), Salt Lake City, UT, September 1993. p 1333–1342

Fejer BG, Kelley MC (1980) Ionospheric irregularities. Rev Geophys 18(2):401–454. https://doi.org/10.1029/RG018i002p00401

Freitas MJS, Moraes A, Marques JC, Rodrigues F (2022) A contribution to real-time space weather monitoring based on scintillation observations and IoT. Adv Space Res 70(2):456–469. https://doi.org/10.1016/j.asr.2022.04.058

Fremouw EJ, Leadabrand RL, Livingston RC, Cousins MD, Rino CL, Fair BC, Long RA (1978) Early results from the DNA wideband satellite experiment—complex-signal scintillation. Radio Sci 13(1):167–187. https://doi.org/10.1029/RS013i001p00167

Jakowski N (1996) TEC monitoring by using satellite positioning systems in Modern Ionospheric Science. In: Ruster R, Schlegel K, Katlenburg-Lindau EGS (eds) H Kohl. ProduServ GmbH Verlagsservice, Berlin, pp 371–390

Jakowski N, Mayer C, Hoque MM, Wilken V (2011) Total electron content models and their use in ionosphere monitoring. Radio Sci. https://doi.org/10.1029/2010RS004620

Jiao Y, Morton YT (2015) Comparison of the effect of high-latitude and equatorial ionospheric scintillation on GPS signals during the maximum of solar cycle 24. Radio Sci 50:886–903. https://doi.org/10.1002/2015RS005719

Komjathy A, Yang Y-M, Meng X, Verkhoglyadova O, Mannucci AJ, Langley RB (2016) Review and perspectives: understanding natural-hazards-generated ionospheric perturbations using GPS measurements and coupled modeling. Radio Sci 51:951–961. https://doi.org/10.1002/2015RS005910

Ledvina BM, Powell SP, Kintner PM, Psiaki ML (2003) "A 12-channel real-time GPS L1 software receiver1," proceedings of the 2003 national technical meeting of the institute of navigation, Anaheim, CA, January 2003. p 767–782.

Mitchell CN, Spencer PSJ (2003) A three-dimensional time-dependent algorithm for ionospheric imaging using GPS. Ann Geophys 46(4):687–696

Moraes AO, Vani BC, Costa E, Sousasantos J, Abdu MA, Rodrigues F et al (2018) Ionospheric scintillation fading coefficients for the GPS L1, L2, and L5 frequencies. Radio Sci 53:1165–1174. https://doi.org/10.1029/2018RS006653

Nishioka M, Tsugawa T, Kubota M, Ishii M (2013) Concentric waves and short-period oscillations observed in the ionosphere after the 2013 Moore EF5 tornado. Geophys Res Lett 40:5581–5586. https://doi.org/10.1002/2013GL057963

O'Hanlon BW, Psiaki ML, Powell S, Bhatti JA, Humphreys TE, Crowley G, Bust GS (2011) "CASES: A smart, compact GPS software receiver for space weather monitoring," proceedings of the 24th international technical meeting of the satellite division of the institute of navigation (ION GNSS 2011), Portland, OR, September. p 2745–2753

Okoh D, Obafaye A, Rabiu B, Seemala G, Kashcheyev A, Nava B (2021) New results of ionospheric total electron content measurements from a low-cost global navigation satellite system receiver and comparisons with other data sources. Adv Space Res 68(9):3835–3845. https://doi.org/10.1016/j.asr.2021.07.018

Portella IP, de Moraes AO, da SilvaPinho M, Sousasantos J, Rodrigues F (2021) Examining the tolerance of GNSS receiver phase tracking loop under the effects of severe ionospheric scintillation conditions based on its bandwidth. Radio Sci. https://doi.org/10.1029/2020RS007160

Rodrigues FS, Moraes AO (2019) ScintPi: a low-cost, easy-to-build GPS ionospheric scintillation monitor for DASI studies of space weather, education, and citizen science initiatives. Earth Space Sci 6:1547–1560. https://doi.org/10.1029/2019EA000588

Rodrigues FS, Socola JG, Moraes AO, Martinis C, Hickey DA (2021) On the properties of and ionospheric conditions associated with a mid-latitude scintillation event observed over southern United States. Space Weather. https://doi.org/10.1029/2021SW002744

Septentrio (2022) PolaRx5S Reference Guide, Septentrio, Greenhill Campus, Interleuvenlaan 15i, B-3001 Leuven, Belgium, August 19, 2022. p 1-503. https://www.septentrio.com/en/products/gnss-receivers/reference-receivers/polarx5s

Skone S, Knudsen K, de Jong M (2001) Limitations in GPS receiver tracking performance under ionospheric scintillation conditions. Phys Chem Earth Part A Solid Earth Geodesy 26(6–8):613–621. https://doi.org/10.1016/S1464-1895(01)00110-7

Stubbe P, Hagfors T (1997) The Earth's ionosphere: a wall-less plasma laboratory. Surv Geophys 18:57–127. https://doi.org/10.1023/A:1006583101811

Tsurutani BT, Verkhoglyadova OP, Mannucci AJ, Lakhina GS, Li G, Zank GP (2009) A brief review of "solar flare effects" on the ionosphere. Radio Sci. https://doi.org/10.1029/2008RS004029

Valladares CE, Chau JL (2012) The low-latitude ionosphere sensor network: initial results. Radio Sci. https://doi.org/10.1029/2011RS004978

Valladares CE, Hei MA (2012) Measurement of the characteristics of TIDs using small and regional networks of GPS receivers during the campaign of 17–30 July of 2008. Int J Geophys. https://doi.org/10.1155/2012/548784

Valladares CE, Basu S, Groves K, Hagan MP, Hysell D, Mazzella AJ, Sheehan RE (2001) Measurement of the latitudinal distributions of total electron content during equatorial spread F events. J Geophys Res 106(12):29133–29152. https://doi.org/10.1029/2000JA000426

Vani BC et al (2019) A novel approach to improve GNSS precise point positioning during strong ionospheric scintillation: theory and demonstration. IEEE Trans Veh Technol 68(5):4391–4403. https://doi.org/10.1109/TVT.2019.2903988

Vani BC, Moraes AO, Salles LA, Breder VHF, Freitas MJS, Monico JFG, de Paula ER (2021) Chapter 13—Monitoring ionospheric scintillations with GNSS in South America: scope, results, and challenges. In: Srivastava PK, George PP (eds) GPS and GNSS Technology in Geosciences. Elsevier, Amsterdam

Verhulst TGW, Stankov SM (2020) Height dependency of solar eclipse effects the ionospheric perspective. J Geophys Res Space Phys. https://doi.org/10.1029/2020JA028088

Wright I, Solanki I, Desai A, Socola JG, Rodrigues FS (2022) Autonomous platform for distributed ionospheric studies and citizen science initiatives, presented at the 2022. CEDAR Workshop, Austin USA

Yeh KC, Liu C-H (1982) Radio wave scintillations in the ionosphere. Proc IEEE 70(4):324–360. https://doi.org/10.1109/PROC.1982.12313

Zhang S-R, Erickson PJ, Vierinen J, Aa E, Rideout W, Coster AJ, Goncharenko LP (2021) Conjugate ionospheric perturbation during the 2017 solar eclipse. J Geophys Res Space Phys. https://doi.org/10.1029/2020JA028531
Zhang L, Morton YT (2009) Tracking GPS signals under ionosphere scintillation conditions, proceedings of the 22nd international technical meeting of the satellite division of the institute of navigation (ION GNSS 2009), Savannah, GA, September 2009. p 227–234

Publisher's Note